# Precise Phase Calibration of a Controlled Reception Pattern GPS Antenna for JPALS

Ung Suok Kim, David S. De Lorenzo, Jennifer Gautier, Per Enge
Stanford University
Dennis Akos
University of Colorado at Boulder
John Orr
Worcester Polytechnic Institute

***Abstract-* The Joint Precision Approach and Landing System (JPALS) is being developed to provide navigation to support aircraft landings for the U.S. military. One variant of JPALS is the Shipboard Relative GPS (SRGPS), which will be implemented on an aircraft carrier. In order to meet strict accuracy, integrity, continuity, and availability goals in the presence of hostile jamming and in a harsh multipath environment, advanced technologies are required. One of those being studied is a controlled reception pattern antenna (CRPA) array with beam steering/adaptive null forming capabilities.**

**The Stanford University GPS Laboratory has developed a software tool to study CRPA algorithms and their effects on GPS signals and tracking characteristics. A testbed has been constructed to investigate hardware issues including the phase center stability of the antenna elements and mutual coupling effects. This testbed consists of a 3 element antenna array with a baseline of 1 meter, using high-quality survey-grade or lower-quality patch antennas. Data has been taken using this array in conjunction with sufficient satellite constellation and antenna array motion to ensure complete azimuth and elevation signal coverage. A carrier phase-based attitude determination algorithm was used to generate inter-antenna bias residuals, allowing characterization of the virtual phase center of the array. Repeating the testing procedure both with survey-grade antennas, for which the phase center characteristics are well known, and with a patch antenna possessing unknown phase center behavior, allows characterization of the azimuth- and elevation-dependent properties of the patch antenna phase center. In addition, mutual coupling effects have been investigated by adding inactive patch elements around the active patch antenna. All results are compared to predictions from detailed simulation of the patch antenna used using an EM modeling software package.**

## I. INTRODUCTION

JPALS is a system being developed to provide navigation to support landings for U.S. military aircraft. There are two main variants of JPALS being pursued. The system being developed for the Air Force is called the Land-based Differential GPS (LDGPS). The other variant, being developed for the Navy, is called the Shipboard Relative GPS (SRGPS). The SRGPS will be implemented on an aircraft carrier, and should provide sufficient accuracy, integrity, continuity, and availability to allow automatic landings in zero visibility conditions under a multitude of operating conditions. Some of these operating conditions can be extremely demanding as service must be available even in the presence of hostile jamming, and a harsh multipath environment at the reference antenna location on the mast arm of the island superstructure.

Currently performance specifications call for a vertical accuracy of 0.2 meters, with a vertical alarm limit (VAL) of 1.1 meters. The integrity requirement is that the probability of hazardously misleading information (HMI) must be $10^{-7}$ per approach, and the system must be available 99.9% of the time under normal conditions. In addition, the system must be able to continuously provide service with greater than 95% availability even with hostile jamming present [1]. In order to meet such stringent performance requirements, SRGPS will be a dual frequency carrier-phase differential GPS system for which an accurate tracking of the carrier phase is critical for a precise position solution. In addition, a number of advanced technologies are being pursued. One of these is a Controlled Reception Pattern Antenna (CRPA) with beam steering / adaptive null forming capabilities. For any new technology being considered for SRGPS, such as CRPAs, its exact effect on the carrier-phase of the measurement must be characterized and minimized, and its contribution to the integrity and error budget must be known.

The Stanford GPS laboratory has developed a software tool to study CRPA algorithms. However, in order to have a useful software tool, all relevant hardware issues must be included in the simulation. At present the effects of both mutual coupling within the array and of signal combining for beam/null steering on the effective phase center for each received satellite signal is not well understood [2]. To address this problem, we are beginning with an Electromagnetic CAD model of a typical patch antenna, and then expanding to models of 2 X 2 and 3 X 3 arrays of these elements. Use of a full finite element simulation of the three-dimensional structure enables calculation of the received signal magnitude and phase at each element as a function of signal direction of arrival. This approach takes into account both the phase center motion of each element as direction of arrival varies, and the coupling effects among elements. The approach is being validated with test antenna elements fabricated to match the electromagnetic CAD model. The software package used was Ansoft's HFSS (High Frequency Structure Simulator)

A testbed has been constructed to characterize the elevation and azimuth dependent phase center offsets of the antenna elements and the mutual coupling effects between them. The testbed consists of a three-element antenna array with baselines of 1 meter. A carrier phase-based attitude determination algorithm will be used to determine the inter-antenna line bias residuals. A data set taken using very stable survey-grade antennas should provide an initialization for each line bias, and should show no dependence on the azimuth and elevation of the received signal. By substituting one of the survey-grade antennas with a lower quality patch antenna, the line bias residuals will be dominated by the phase center behavior of the substituted antenna. In addition, by adding non-active antenna elements around the substituted patch antenna in an array configuration, the mutual coupling effects of these non-active elements on the active patch antenna can be seen.

## II. Test Set-Up

### *A. Hardware Testbed*

Fig. 1 shows a schematic diagram of the hardware testbed setup. A sturdy three-element antenna array was constructed using thick aluminum U channel beams to eliminate any kind of flexure or movement that could corrupt the baseline lengths. The antenna elements are in an equilateral triangular

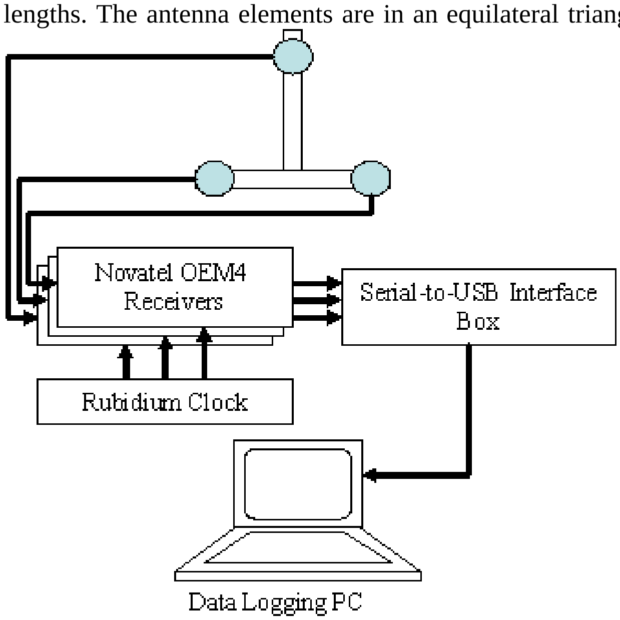


Fig. 1. Hardware Testbed Data Flow

configuration with one meter baseline lengths. The high quality survey-grade antennas used to initialize the line biases are the Novatel GPS 700 pinwheel antennas which have a very stable phase center. Three different antennas will be substituted and tested on the array (Fig. 2): a Novatel GPS 501 antenna, a Micropulse Mini-arinc 12700 antenna, and a rectangular patch antenna with a center frequency at L1 constructed at the Stanford GPS lab. The decision was made to construct our own antenna because of the difficulty we faced in obtaining detailed design information on any commercially available antennas, and precise design information was absolutely essential to getting meaningful results from an accurate simulation in HFSS. Mutual coupling effects will be studied using 2x2 half wavelength spaced rectangular four-element array using the Micropulse Mini-arinc antennas and the constructed patch antennas. Only the constructed patch antenna array will be simulated in HFSS and results compared to actual data collected.

a) b)

Fig. 2.a). Antenna array shown with constructed single patch antenna
b). Novatel OEM4 receivers and data logging PC

The signals from each of the three antennas go into three Novatel OEM4 receivers, which are running off a common rubidium clock (Fig. 2). The receivers are connected to a data collecting PC via a serial-to-USB interface box, and the PC logs data from all three receivers.

### *B. Ansoft's HFSS*

The premise behind any numerical EM methods is to find approximate solutions to Maxwell's equations (or equations derived from them) that satisfy the boundary and initial conditions given by the problem. Numerical methods fall into two broad categories: frequency domain and time domain. One of the most prominent 3D frequency domain methods in use is the finite element method (FEM), which Ansoft's HFSS (High Frequency Structure Simulator) incorporates. The primary unknown being solved for in FEM is usually a field or a potential, and this field domain is discretized rather than the boundary surfaces. For 3D problems, the field is discretized into tetrahedral volume elements, which provides maximum flexibility in defining arbitrary geometries.

As mentioned above, one of the greatest strengths of FEM lies in its generality. In addition to the ease in which geometries are defined, an error-based iterative automatic mesh refinement is a function unique to FEM. However, FEM is not without its drawbacks. Because the field domain is discretized, rather than some boundary surface, a complete volume must be discretized, resulting in large problem sizes [3]. Table 1 lists some of the pros and cons of FEM solvers such as HFSS.

TABLE 1
Pros And Cons Of 3D FEM Solvers

| Pros | Cons |
|---|---|
| Easy to draw arbitrary geometries and structures. | Must discretize entire field volume leading to large problem size. |
| Multimode S-parameters available. | Wave ports occupy complete "face." |
| Error-based iterative automatic mesh refinement. | Must approximate free space with Absorbing Boundary Conditions (ABCs) or Perfectly Matched Layers (PMLs), resulting in longer computing time. |
| Functional visualization of results: large number of plot types. | |

After reviewing a number of commercially available EM software packages, including some Method of Moments solvers, we decided to go with Ansoft's HFSS for three major reasons: 1) we needed a full 3D numerical field solver; 2) the automatic mesh generation feature greatly simplified the problem set-up and generation; 3) HFSS has a flexible parametric solver feature that facilitates precise tuning of certain design parameters.

## III. EXPERIMENTAL PHASE-CENTER DETERMINATION

Differential phase-center calibration of a multi-element GPS antenna array utilizes a simple modification to the basic measurement equations of GPS-based multi-antenna attitude determination [4,5].

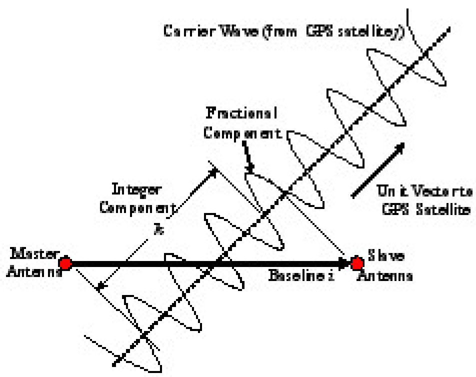


Fig. 3. Attitude determination – 2-D development

### A. Fundamentals of GPS-Based Attitude Determination

The fundamentals of GPS attitude determination are well covered in the literature, with [6] being the standard reference. Consequently, a rather brief overview is all that will be required in order to introduce the changes necessary for differential phase-center calibration [adapted from 6].

In two dimensions, the determination of orientation by using measurements of the phase of incoming plane waves proceeds logically (Fig. 3 – the index $i$ corresponds to baseline and $j$ corresponds to satellite). Two antennas, by convention labeled "master" and "slave", define a baseline $b$ coordinatized in a body-fixed basis. The carrier wave from a far-distant source, in this case a GPS satellite, is incident at each antenna; accurate measurement of the arrival phase $f$ is made simultaneously (or nearly so) at each antenna. The precise distance to the GPS satellite, and hence the exact whole number of carrier wavelengths, is not known without additional processing of the GPS signals (e.g., L1/L2 processing); this whole number ambiguity can be treated as a random integer while lock is maintained. By taking the single-difference between the phase-plus-integer value at each antenna for several satellites ($?f + k$), the orientation $A$ (a 3x3 transformation matrix) between the body-fixed basis and the external reference system can be found. In addition, there may be some differential line bias, signal delay, or measurement asynchrony $B$ between the signals measured at each receiver, as well as measurement noise ?. The addition of a third antenna, defining a second baseline noncolinear with the first, allows a straightforward extension to three dimensions:

$$\Delta r_{ij} \equiv \left(\Delta j_{ij} + k_{ij}\right) l = \vec{b}_i^T A \hat{s}_j + B_i + n_{ij} \qquad (1)$$

Normal multi-antenna 3-D GPS attitude processing operates epoch-by-epoch according to (1) with the final product being an attitude transformation matrix between the external basis (e.g. ENU) and the body-fixed basis, as well as the antenna line biases. The phases of the incoming carrier wave signals at each of the antennas are measured, satellite ephemerides are decoded from the navigation message, and baseline geometry is available from previous survey or calibration. Given knowledge of the number of integer wavelengths along each baseline for each satellite in view, (1) is solved by, for example, least-squares minimization of an appropriate cost-function [7] or deterministic (closed-form) attitude and bias updates [8].

### B. Changes to Measurement Equation for Differential Phase-Center Calibration

With a simple modification to the measurement equation (1), it is possible to use natural satellite constellation motion and planned reorientation of the antenna array to determine the azimuth- and elevation-dependent differential phase delay along each antenna baseline. For this application, accurate knowledge of the body-to-ENU transformation matrix $A$ is required, based either on *a priori* survey data or on a converged attitude solution. Given this knowledge, it should be apparent that all terms in (1) are known with the exception of the integers $k_{ij}$ and the differential biases $B_i$. This leads to a natural reformulation as follows:

$$k_{ij} - B_i / l = -\Delta j_{ij} + \left(\vec{b}_i^T A \hat{s}_j\right) / l \qquad (2)$$

Now it is possible to exploit the fact that the $k_{ij}$ are integers: the bias estimates $B_i$ are those values that, when added to each element on the right-hand-side of (2), leave numbers that are as close as possible, on average, to integers. The residual of $B_i$ for each of the integers $k_{ij}$ is the differential phase-center contribution from satellite $j$ (with signal arrival direction at azimuth $a_j$ and elevation $?_j$) on baseline $i$. Including this term $dB_{ij}$ yields the following basic relation for differential phase-center calibration:

$$\left(\Delta j_{ij} + k_{ij}\right) l = \vec{b}_i^T A \hat{s}_j + B_i + \underline{dB_{ij}\left(a_j, z_j\right)} + n_{ij} \qquad (3)$$

Accurate calculation of the $dB_{ij}$ does require the assumption that the differential phase-center motion is small compared to a carrier wavelength yet large compared to measurement noise. Calculation also depends, in practice, on using a running average for the line bias estimates, say over a period of approximately 1-hour, such that the effects of measurement noise and unbalanced satellite sky coverage do not introduce excessive prejudice on the calculation of $dB_{ij}$ at each epoch. Further, the goal is to utilize sufficient data collection time so that sky coverage is, on average, nearly balanced with respect to signal arrival direction.

### C. *Experimental Results*

A 3-element array of NovAtel pinwheel antennas defining 1.0m equilateral baselines was placed on the roof of a building on the Stanford University campus. GPS data packets including pseudorange, carrier phase, and satellite ephemerides were collected on several occasions, and then post-processed according to (3). Data from 03 Mar. 2004 and 07 Mar. 2004 (each dataset representing 24 hours of data at 0.2Hz) were used to produce complete differential phase-center maps along each array baseline (Fig. 5). Note that a reorientation of the array (the 2nd test date) is required in order to produce complete azimuth and elevation sky coverage due to the inclined orbits of the GPS satellites.

As a further check on the algorithms and methods needed to implement (3), the data from several separate test dates were compared for consistency in their differential phase-center estimates – this is because “truth” data were not available, e.g., from anechoic chamber testing. Pairs of data records utilized the same antenna elements, geometry, and site, but incorporated a realignment of the array to isolate environmental or multipath effects. This allowed comparison between the differential phase-center predictions obtained from 3 pairs of test dates for data along baseline #1 (there was an alignment change on one of the antenna elements for the second baseline on the latter test dates). The mean root-mean-squared difference between the estimates from each test date for baseline #1 was 0.018?; this is compared to a functional range of phase-center values for these baselines of 0.09?. Furthermore, estimates derived on the 2nd test date of each pair agreed within one standard deviation of those from the 1st test date for 84% of the azimuth/elevation pairs; this number went up to 97% for agreement within two standard deviations. The median value of the standard deviation was 0.017?.

Qualitatively, the shape of the differential phase delay functions was preserved between test dates; for example, at an azimuth of 225° the differential phase-center predictions for baselines #1 and #2 may be plotted, along with the standard deviations on the phase-center estimates (Fig 6). Therefore, the differential phase-center prediction method described above is repeatable.

### D. *Extension to Method for Phase-Center Calibration*

So far, a method has been introduced to calculate the ***differential*** phase delay between two antennas defining a baseline. Of further interest is to extend the current method to allow phase-center calibration of a single antenna. This process leverages the assumption that the general structure of each antenna’s phase-center map is preserved under antenna realignment within the multi-element array.

The phase-center map can be thought of as a 2-D surface parameterized by azimuth and elevation and invariant with respect to a basis fixed in the antenna. The differential phase-center $dB_i$ that was calculated previously can be treated as the difference between the individual phase-center characteristics of each antenna along that baseline. Here the subscript *j* has been dropped for convenience, *?ß* is introduced as the notation for the phase-center structure of a single antenna, and the subscripts *A* and *B* reference the antennas along baseline *i*:

$$dB_i(a,z) = \partial b_A - \partial b_B \tag{4}$$

Clearly, there is no way to decompose the calculation of $dB_i$ into its separate elements $?ß_A$ and $?ß_B$ with measurements made using only a single experimental setup. However, if one of the antennas is reoriented within the array, and this transformation *R* is known, then differential phase-center calibration $dB_i$’ of this new array does allow recovery of the individual phase delay maps for antennas *A* and *B*.

$$\begin{aligned} dB_i(a,z) &= \partial b_A - \partial b_B \\ dB_i'(a,z) &= \partial b_A - R\partial b_B \end{aligned} \tag{5}$$

## IV. MUTUAL COUPLING

When two antennas are close to each other, some of the energy that is associated with one antenna (in either the transmit or receive modes) ends up at the other. This interchange of energy is known as mutual coupling, and there are many mechanisms through which it occurs. Mutual coupling effects are rather difficult to predict analytically, particularly for patch antennas, but they must be taken into account both for accurate beam/null steering and to accomplish the goals of this paper. The amount of mutual coupling effect seen depends on three main factors: the receiving characteristic of each antenna element, the relative separation between antennas, and the relative orientation of each antenna element.

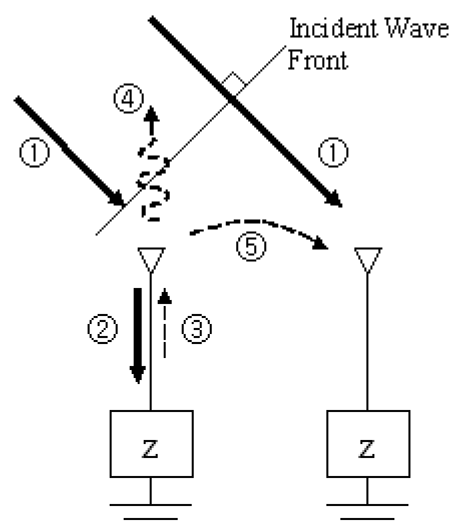


Fig. 4. Mutual Coupling Path in Receiving Antenna Pair

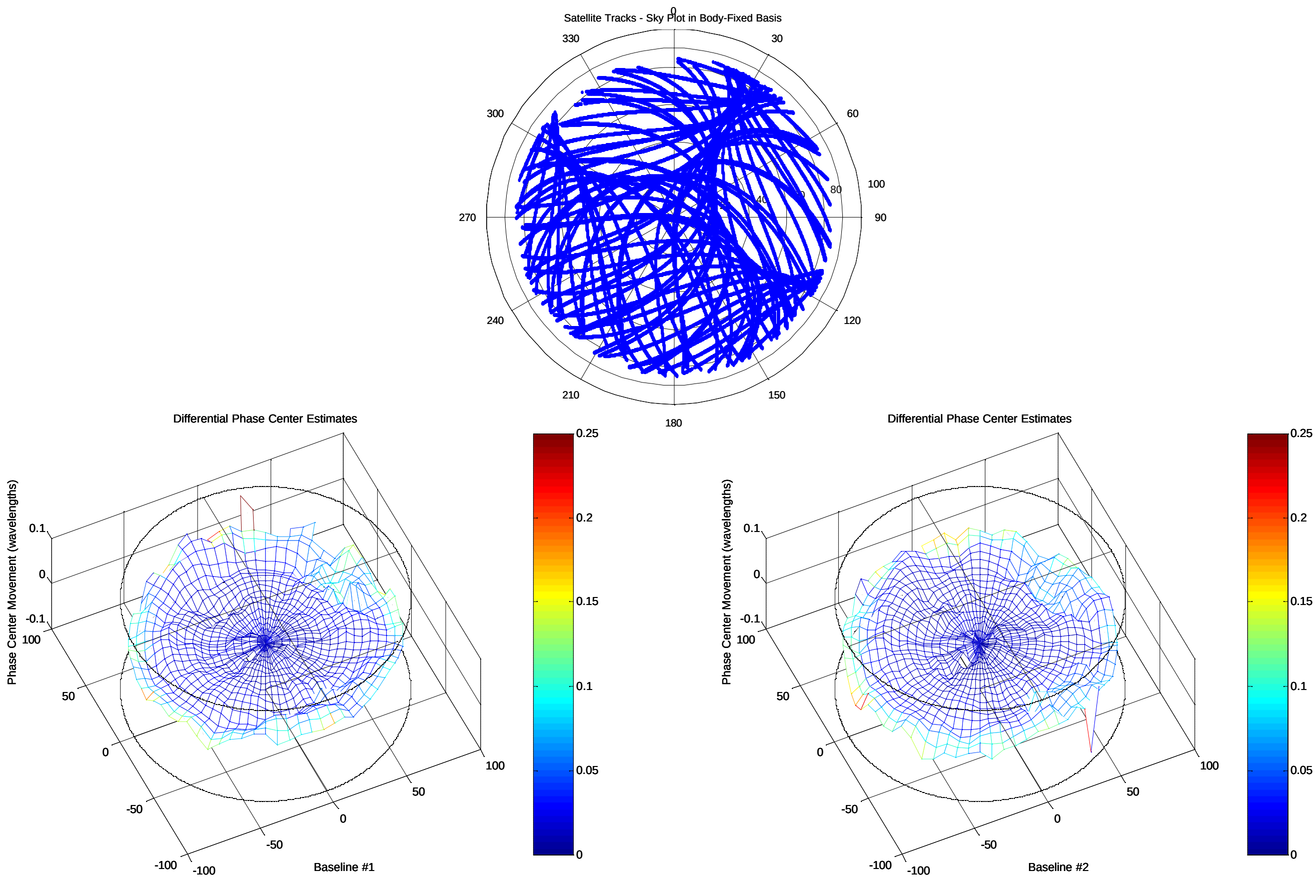


Fig. 5. Differential phase-center maps for baselines #1 (on left) and #2 (on right), as well as satellite sky-tracks, in a body-fixed basis, used in the processing. The level of the contour surface shows the differential phase-center for the antennas along that baseline; the colorbar scales on the right show the standard deviation on the phase-center estimates.

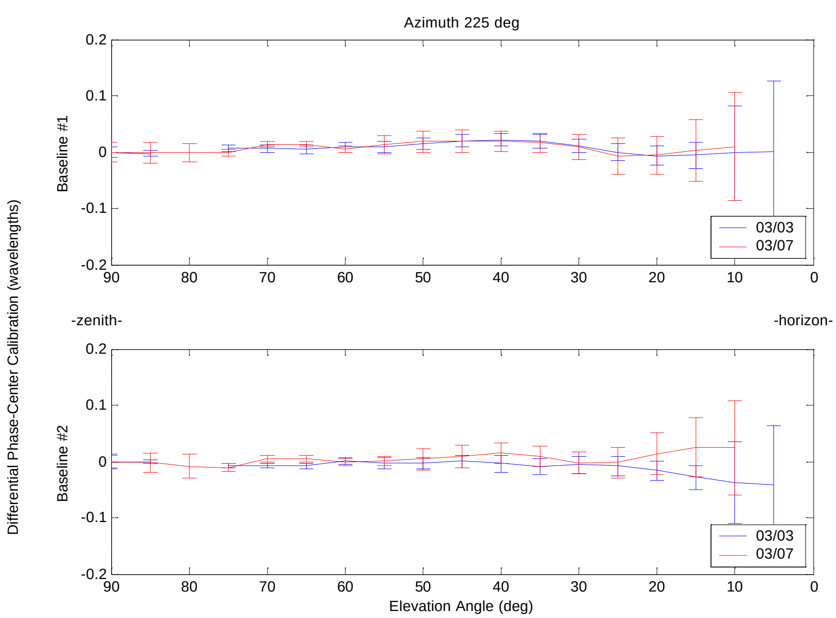


Fig. 6. Differential phase-center predictions from two test dates. Error bars show one standard deviation, which increases near the horizon due to lowered signal SNR and multipath effects

To illustrate the mechanism by which mutual coupling occurs, let us look at two passively loaded antenna elements (Fig. 4). Any incident wave ( ? ) received by the first antenna will impress a current flow in that antenna ( ? ). With an antenna that's well matched to the impedance of the receiver, the current from the antenna ( ? ) will flow unimpeded into the receiver. However, any mismatch in impedance between the antenna and receiver will result in some of the signal being reflected back towards the antenna ( ? ). This reflection results in part of the incident wave being rescattered into space ( ? ), some of which will be directed towards the other antenna ( ? ). The signal received at the second antenna will be a vector addition of the scattered wave from the first antenna ( ? ) and the original incident wave ( ? ). The first antenna will also be subject to mutual coupling effects induced by the scattering wave produced by the second antenna.

For a large array with a sufficient number of antenna elements so that edge effects can be ignored, the relative shape of the antenna pattern will be mostly unchanged with and without coupling interactions. The only effect will be a scaling up or down in amplitude while the shape is preserved. However, for smaller arrays such as we're looking at in this study, the edge effects become more dominant and mutual coupling will affect the antenna pattern [9].

These mutual coupling effects in an array can be represented from an impedance standpoint using standard circuit analysis. Suppose we have an array of N elements. This can be treated as an N port network, giving the following

$$
\begin{aligned}
V_1 &= Z_{11}I_1 + Z_{12}I_2 + \cdots + Z_{1N}I_N \\
V_2 &= Z_{21}I_1 + Z_{22}I_2 + \cdots + Z_{2N}I_N \\
&\vdots \\
V_N &= Z_{N1}I_1 + Z_{N2}I_2 + \cdots + Z_{NN}I_N
\end{aligned}
\tag{6}
$$

where $V_n$ and $I_n$ are the impressed voltage and current in the $n^{th}$ element, and $Z_{nn}$ is the self-impedance of the $n^{th}$ element. The mutual impedance $Z_{mn}$ between elements $m$ and $n$ will be reciprocal (i.e. = $Z_{nm}$), assuming all elements are identical [10]. This is a very straightforward representation of mutual coupling effects. However the impedance terms are rather difficult to obtain. For a transmitting array, each self and mutual impedance terms in (6) can be experimentally measured, but such is not the case for receiving antenna arrays. It is impossible to get independent experimental measurements of each mutual impedance term in the above equation for a receiving array. Thus, mutual coupling effects in receiving arrays must be studied in terms of the overall impedance in each channel.

## IV. Results

### *A. Testbed Results*

Fig. 7 shows the phase center residual results for four different antennas. We are working under the assumption that the Novatel pinwheel 700 antennas have a very stable phase center, and thus any differences seen from the plots shown in Fig. 4 will be attributed to the substituted antenna.

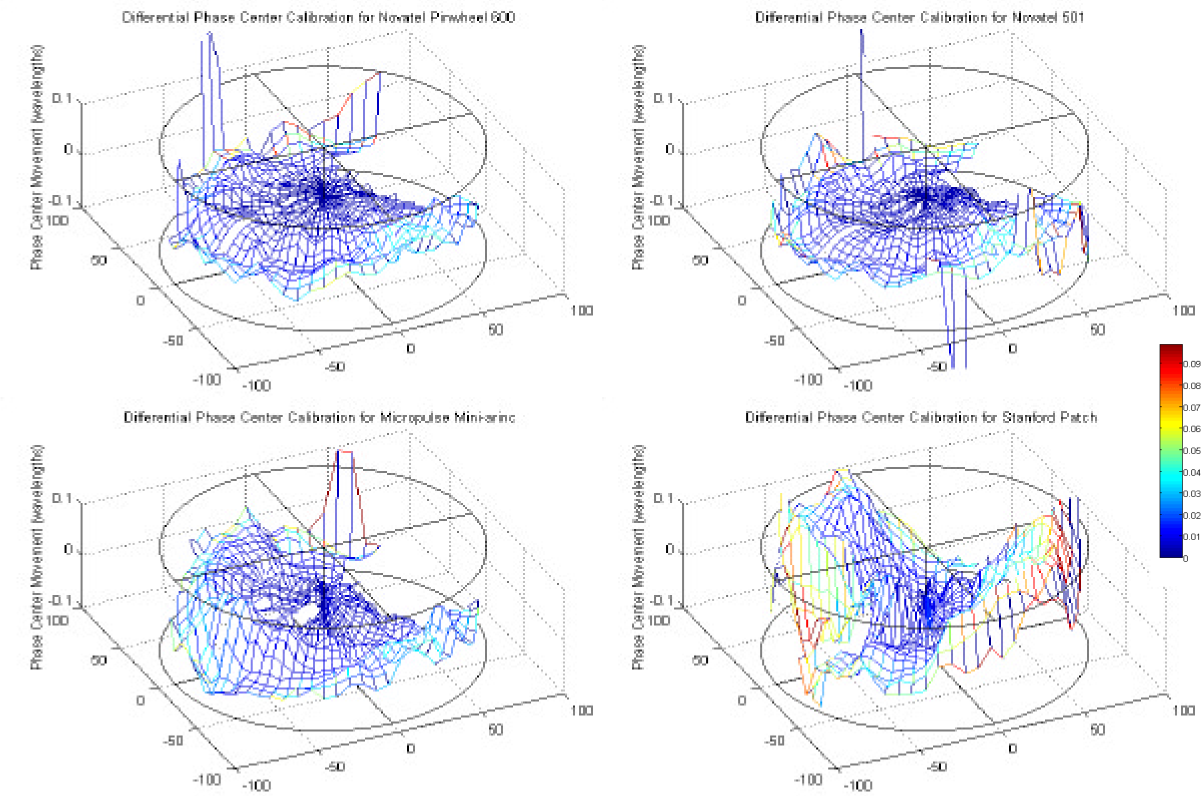


Fig. 7. Phase center movement for different antennas

The first thing to note is the area of noisy phase center residual seen near the horizon that is prevalent in all of the plots in Fig. 7 and also in Fig. 4 at the same location. This is due to multipath errors for signals coming from that direction, and it shows that the rooftop where the data was taken is not a multipath-free environment. The results are shown for four different antennas: Novatel Pinwheel 600 (a predecessor to the 700 model), Novatel 501, Micropulse Mini-Arinc, and the constructed patch antenna. It is interesting to note that the phase center performance is indicative of the quality and cost of each antenna. The pinwheel antenna shows the most stable phase center characteristics. The patch constructed at the Stanford GPS lab does not have any multipath rejecting capabilities near the horizon and this is certainly evident in the plot.

Fig. 8 shows the mutual coupling effects seen from adding more antenna elements around the "active" antenna. This plot shows that the testbed and algorithm developed is able to capture, using live GPS signals, mutual coupling effects introduced by adjacent antenna elements. Note that the amount of mutual coupling effect seen depends greatly on the relative orientation of the antenna elements with respect to the incident signal.

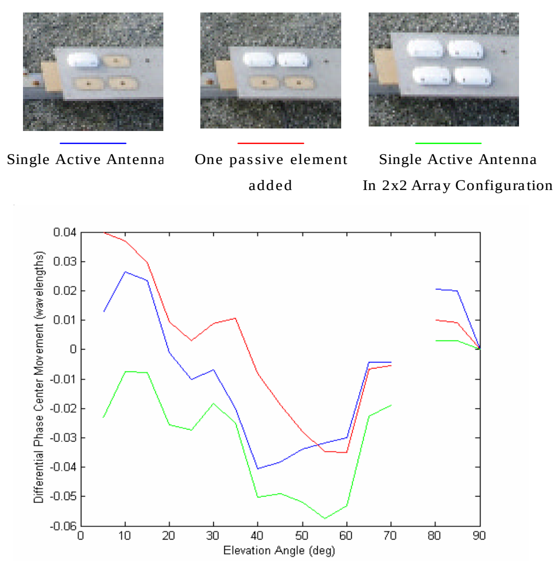


Fig. 8. Mutual coupling effects seen from testbed using Micropulse antennas

*B. Simulation Process and Results*

An understanding of the variation of received signal phase effects (both phase delay and group delay) as a function of angle of incidence for a single patch antenna and for each element in an array of patches is desired. The analytical solution for an accurate 3-D model is not feasible, so numerical simulation is applied using a full three-dimensional finite element solver. In this work, Ansoft HFSS Version 9.1 is used.

In the limiting case of an infinitesimally small receiving antenna, received phase would be independent of angle of incidence. However, this is not the case in general for finite-sized antennas.

Simulation results for two antenna configurations are presented: a single isolated patch and a four-patch array with the patches located one half wavelength apart, above a ground plane. In each case, results are presented for a single patch whose feed is located at the origin of the coordinate system. Table 2 and Fig. 9 define the physical design of the patch.

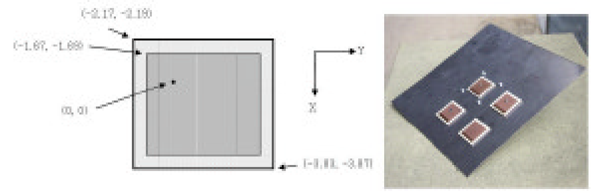

Fig. 9. Constructed patch antenna coordinates and constructed array

TABLE 2
PATCH ANTENNA PARAMETERS

| Parameter | Value |
|---|---|
| Design frequency | 1.57542 GHz |
| Substrate dimensions | 5.5 X 5.56 cm |
| Patch dimensions | 4.5 X 4.56 cm |
| Patch material | copper |
| Feed location | see Fig. 9 |
| Substrate thickness | 0.152 cm |
| Substrate permittivity | 4.5 |
| Substrate material | Rogers TMM |

Fig. 10 shows the comparison between the simulation of the constructed patch, and data obtained from the testbed for the 2x2 configuration seen on both baselines for signals incoming at 0 degree azimuth. The simulation results are referenced to zero at the feed, while the phase residual from the testbed dataset contains an offset that corresponds to the phase of the signal received by the pinwheel antenna in the baseline. This difference is seen as just a constant offset. By removing this offset manually, the basic pattern of the simulated phase center movement can be compared to the data from the testbed. The blue line represents testbed data and the red line is the results from HFSS simulation. The blue error bars represent one standard deviation seen in the test data. The results show good agreement in the middle elevations with deviations seen in the low and high elevation angles. At lower elevations, the discrepancy seen between the testbed data and simulation can be attributed to the low SNR of the GPS signals received, leading to noisier measurements, and possible mulitpath effects seen near the horizon. At higher elevations, we believe the deviation seen is a by product of our algorithm implementation. We discretize the map space by taking 5 degree windows in azimuth and elevation and average out the measurements within that window. At higher elevations, this window starts to become very small, and thus the averaged value is based on much fewer measurements, which can lead to biases.

Fig. 11 shows the mutual coupling effect seen from the simulation of the 2x2 array in HFSS. For the single patch,

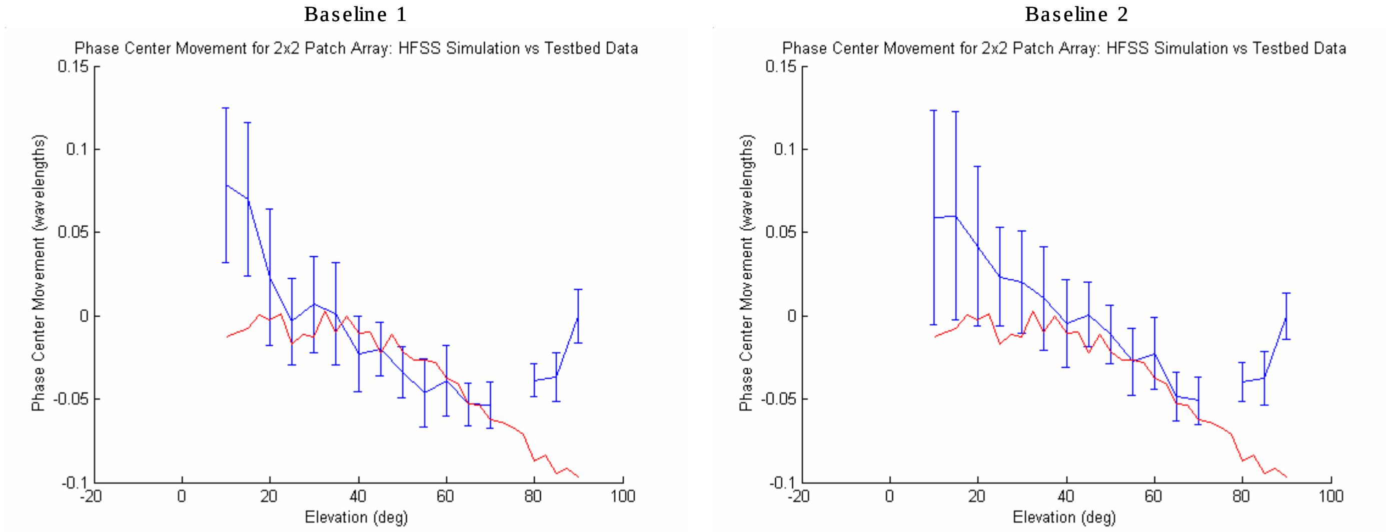


Fig. 10. Comparison between HFSS simulation and testbed data for 2x2 array configuration (data from baseline 1 on the left and baseline 2 on the right)

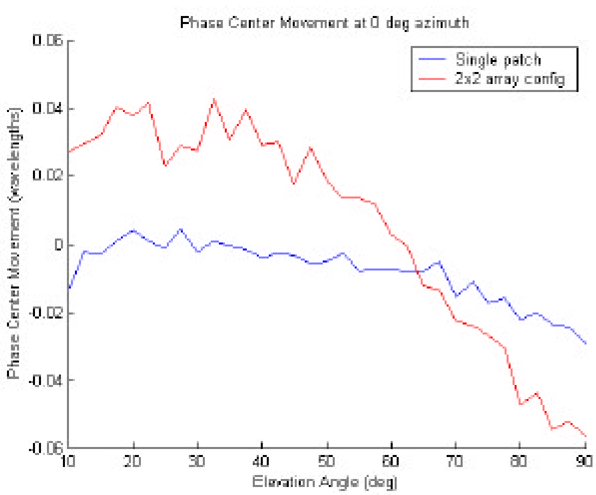


Fig. 11. Mutual coupling effect seen from HFSS simulation of 2x2 array

maximum phase variation is seen to be 12.4 degrees or 0.65 cm at the L1 frequency over the tested range of angles of incidence. For the 2x2 array, the maximum phase deviation is seen to be 35.6 degrees or 1.9 cm for azimuth of zero degrees. These results indicate the effect of mutual coupling among elements in a CRPA array and show that the phase delays are potentially significant, with respect to optimal beam forming as well as to carrier phase tracking and the resulting geometric precision. In all cases, the incident wave is right circularly polarized. The observed point to point variations in the simulation results are primarily the result of the convergence stopping criterion chosen, and will be reduced in further work

## V. CONCLUSIONS

An antenna testbed was constructed at the Stanford GPS laboratory to study hardware-related effects on phase center stability which must be characterized for CRPA applications in JPALS. By using pinwheel antennas with excellent phase stability at two vertices of the triangular test setup, and the antenna under test at the other vertex, the carrier phase residuals, which will be dominated by the antenna under test, can be calculated using a modified attitude determination algorithm. In addition, by adding identical but non-active elements around the antenna under test, we can see the mutual coupling effects introduced by these extra elements. A rectangular patch antenna and array constructed at the Stanford GPS laboratory were tested, and results were compared to simulations from a full 3D finite element-based electromagnetic field solver. These results indicate that phase deviations introduced in arrays of patch antenna elements are potentially significant, and that the modeling approach taken here should permit these effects to be quantified and compensated, at least partially, in beam and null forming algorithm. Also, knowledge of residual phase deviations will be useful in JPALS system performance analysis.

## ACKNOWLEDGMENTS

The authors would like to acknowledge and thank the Naval Air Warfare Center Aircraft Division (NAWCAD) who funded this research.

## REFERENCES

[1] "System Requirement Document for SRGPS" R2 Baseline ver. 1.0, August 2003
[2] Kim, U., Akos, D., Enge, P., and Bastide, F., "Simulation and Validation of a GPS Antenna Array Concept for JPALS Application", *Proceedings ION GNSS 2003*
[3] Swanson, Daniel, "Microwave Circuit Modeling Using Electromagnetic Field Simulation," Artech House, 2003
[4] S. Alban, "Design and performance of a robust GPS/INS attitude system for automobiles," Ph.D. Thesis, Stanford University, expected 2004..
[5] E. Sutton, "Calibration of differential phase map compensation using single axis rotation," Proc. ION GPS-98, pp. 1831-1840, Sept. 1998.
[6] C.E. Cohen, "Attitude determination," *Global Positioning System: Theory and Applications*, B.W. Parkinson and J.J. Spilker, Eds., Reston, VA: AIAA, 1996, pp. 519-538.

[7] D.S. De Lorenzo, S. Alban, J. Gautier, P. Enge, and D. Akos, "GPS Attitude Determination for a JPALS Testbed: Integer Initialization and Testing," *Proc. IEEE PLANS 2004*, in press.

[8] T. Bell, "Global positioning system-based attitude determination and the orthogonal procrustes problem," *J. Guidance, Control, and Dynamics*, vol. 26, no. 5, pp. 820-822, Sept. 2003.

[9] Balanis, Constantine A., "Antenna Theory: Analysis and Design" 2nd edition, John Wiley & Sons Inc., 1997

[10] Stutzman, Warren L., and Thiele, Gary A., "Antenna Theory and Design" 2nd edition, John Wiley & Sons Inc., 1998